BEAM DYNAMICS FOR A PROPOSED RCNP RING CYCLOTRON

T. Yamazaki, K. Hosono, M. Inoue, M. Fuki*, Y. Kadota and I. Miura
Research Center for Nuclear Physics, Osaka University
Mihogaoka Ibaraki, Osaka 567, JAPAN

Abstract

For a proposed RCNP ring cyclotron the focusing property, the stability limit, the deformation of radial phase space through resonance, the variation of energy spread and the phase compression effect of the accelerated beam are studied using measured field data from a model magnet and modified field data. The nonlinear effects of particle motion are investigated using static phase plots.

Introduction

The proposed RCNP accelerator system consists of two ring cyclotrons and an injector cyclotron.[1] The design of the first ring cyclotron (4 sectors, r(inj) = 135 cm, R(ext) = 340 cm, K = 230) was made to provide energies up to 190 MeV and 56 MeV/amu for protons and light ions, respectively. By using a 1/3.5-scale model magnet with trim coils, various magnetic field properties and orbit analyses have been studied for the first ring cyclotron.[2]

Some modifications to the original design for the first ring cyclotron have recently performed in order to provide the acceleration of protons up to 300 MeV.[3] The magnetic field for the high energy version has been designed by increasing the azimuthal width of the magnet with increasing radius. An artificial field for the spiral-sector magnet was generated by correcting the measured field of the straight-sector model magnet and was used for orbit analyses. Recently the 1/3.5-scale straight-sector model magnet has been converted to the new spiral-sector model magnet, and studies on field characteristics and orbit analyses by using revised model magnet are in progress.

Generation of Artificial Field Distribution

A computer code FIGER was developed to generate artificial magnetic field distributions of the ring cyclotron. The measured values are fitted by an analytical expression by the least square methods. The effective field boundary and the fringing field are parameterized and given as inputs of the code FIGER. The artificial magnetic fields are calculated for the mesh points on the polar coordinates. The effect of the fringing-field overlapping is also taken into account for neighbouring magnets. The betatron frequencies ν_R and ν_Z are calculated numerically for the measured field and the

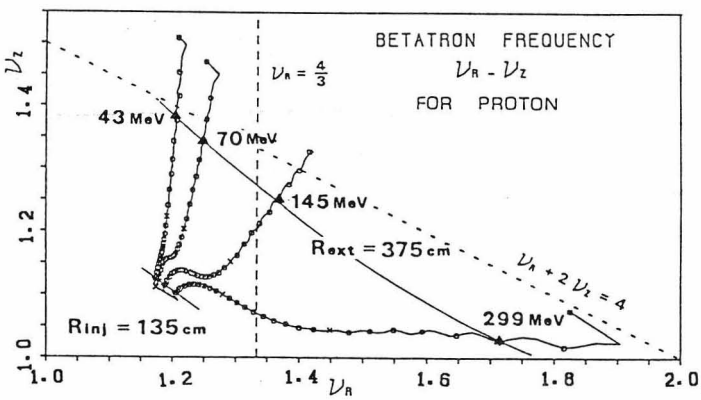

Fig. 1. Betatron frequencies ν_r and ν_z for various operation modes for proton are shown from injection radius 135 cm to extraction radius 375 cm.

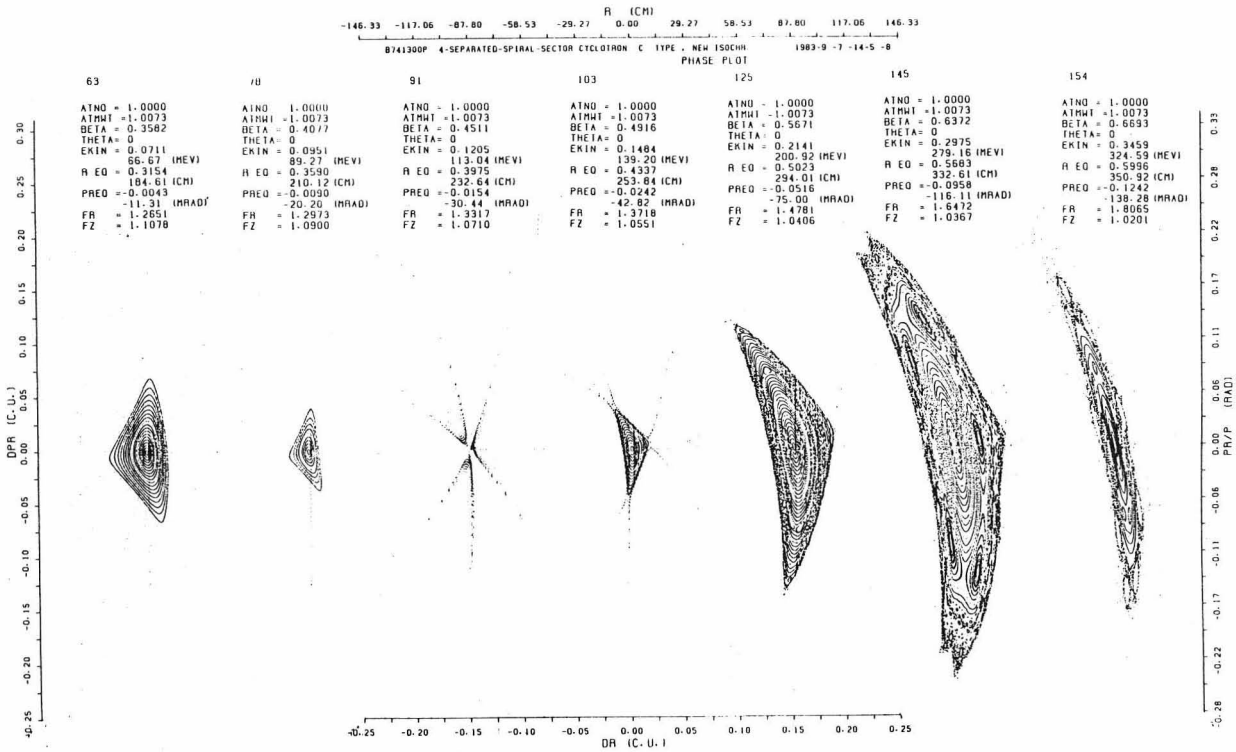

Fig. 2. Phase plots of the proton beams.

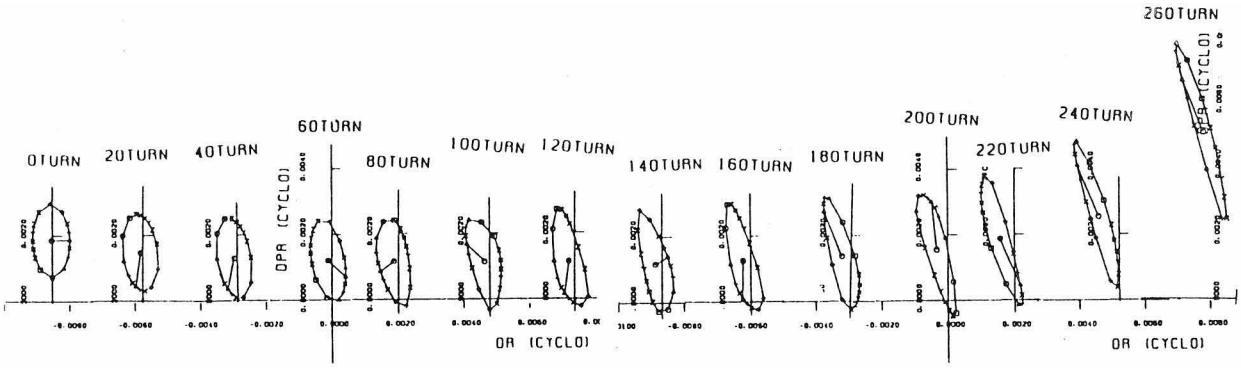

Fig. 3. Radial phase space patterns, observed at an azimuthal angle 0°, are shown in every 20 turns.

corresponding artificial field from injection radius through extraction radius. These results show extremely good agreement. This calculating method is applied to the spiral sector magnet of the first ring cyclotron.

Orbit Properties

The isochronous fields for various particles and energies are used to study the orbit properties of the beams with and without acceleration. The computed betatron frequencies (ν_r and ν_z) of protons are shown in Fig. 1. At extraction radius 375 cm, protons can be accelerated up to 300 MeV. The proton beams are accelerated through ν_r = 4/3 resonance. The phase plots across the ν_r = 4/3 resonance are shown in Fig. 2. The phase plots show triangular shape around the equilibrium orbit and show the existence of ν_r = 4/3 resonance.

The orbit properties of accelerated beams are analyzed. The injection radius and extraction radius are 135 cm and 375 cm, respectively. A constant acceleration voltage 1.0 MV/turn is assumed for the calculation. The azimuthal angle 0° is chosen on the valley center at injection radius. Two RF cavities are located at the angles of 90° and 270°. The radial momentum of the beams without acceleration is zero at valley center of the radial sector. The beam on the phase ellipse is oscillated around the equilibrium orbit with acceleration.

The phase ellipse traced from injection to extraction is plotted in Fig. 3. The beam emittance of the eigen ellipse is 50 mm·mrad at injection radius, and the beam is accelerated with a constant voltage 1 MV/turn. Particles cross the resonance of the ν_r = 4/3 between 60 and 80 turns. The phase ellipse is slightly deformed in crossing this resonance as shown in the figure. Turn separation at the extraction radius is 4.2 mm.

As shown in Fig. 3, the proton beam can pass the ν_r=4/3 resonance in normal acceleration condition. But if a constant acceleration voltage 200 kV/turn is assumed as the extreme acceleration condition, the shape of phase ellipse is deformed considerably after passing through ν_r=4/3 resonance as shown in Fig. 4. The variation of the phase ellipse in the case of a wrong matching condition at injection is shown in Fig. 5. The beam emittance at the injection and the acceleration voltage are the same as that of Fig. 4, but the beam is injected to the point 12 mm different radially from the equilibrium orbit. Both the beam position and the radial momentum oscillate, and the phase ellipse near the extraction radius shows a large deformation.

An acceleration cavity has been studied by using a full-scale model of the cavity, and the voltage

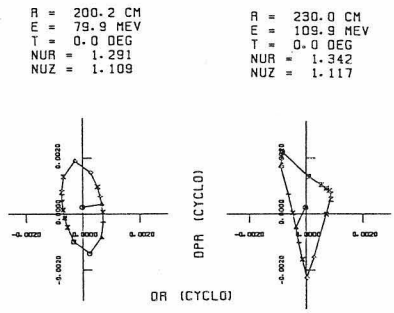

Fig. 4. Radial phase space pattern is deformed after passing through ν_r=4/3 resonance, if low acceleration voltage (200 kV/turn) is assumed in the calculation. The left figure shows the phase space pattern before resonance and the right figure shows after resonance.

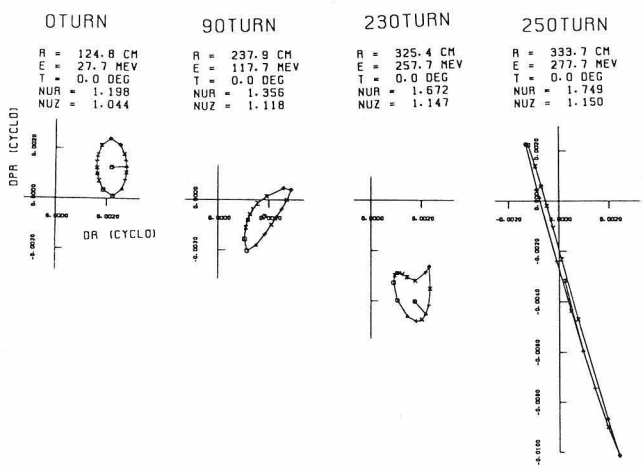

Fig. 5. Radial phase space pattern in the case of a wrong matching condition at injection.

distributions along acceleration gap were measured.[4] Accelerated orbits were calculated by assuming the voltage distribution shows in Fig. 6, where the phase compression effect is also shown. The beams injected with RF phase width 5.7° is accelerated, and at the extracted radius the phase is compressed to RF phase width 1.6°. This ratio corresponds well with the ratio of accelerating voltage at injection and extraction radius.

Phase Plots

The nonlinear effects of particle motion are investigated using static phase plots.

Fig. 7 shows the phase plots of the stable region for protons at large radius for a spiral ring

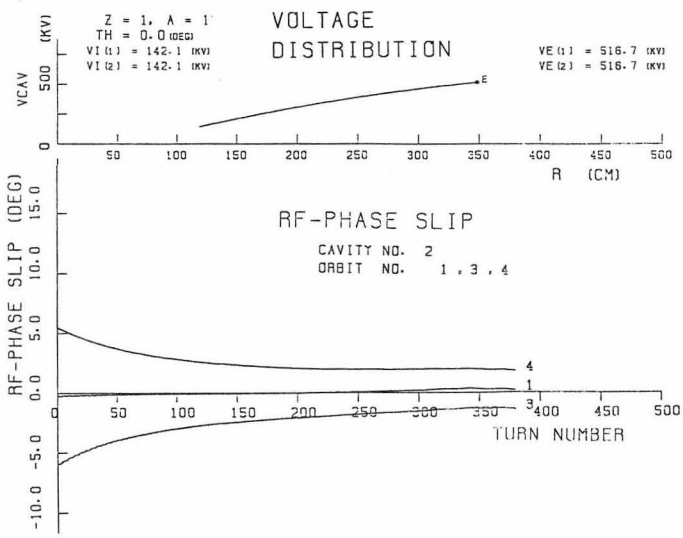

Fig. 6. The voltage distribution of cavities and the RF phase slip of beam show the phase compression of the accelerated beam by RF magnetic field effect.

cyclotron with four magents. Outer eight islands are due to the stable fixed points of ν=12/8 and inner five islands are due to the stable fixed points of ν=8/5. Many small islands are due to higher order fixed points. These islands are surrounded by random plots in higher energy and outer region. The phase plots show stochastic behavior for the orbits apart from the equilibrium orbit. These phase plots are obtained for two types of isochronization (isochronous field with circular approximation and orbital-shape approximation). The size of the stable region for orbital-shape approximation is larger than that for circular approximation. Fig. 8 shows the phase plots near extraction radius. The size of the stochastic region becomes larger at higher energy, and the stable region disappears at 354.3 MeV. These phase plots give global characteristics on orbit stability.

Fig. 9 shows the phase plots of protons at large radius for a straight-sector ring cyclotron with four sector magnets. The magnetic field at larger radius is slightly lower than isochronism. Three islands are appeared, and there is ν_r=4/3 resonance near 188 MeV. These phase plots are similar to those of ν_r=3/3 resonance for three-sector AVF cyclotron near extraction radius.

In some phase plots the large islands are surrounded by small islands and these small islands are surrounded by very small islands. Fig. 10 shows a typical example of the complicated phase plots.

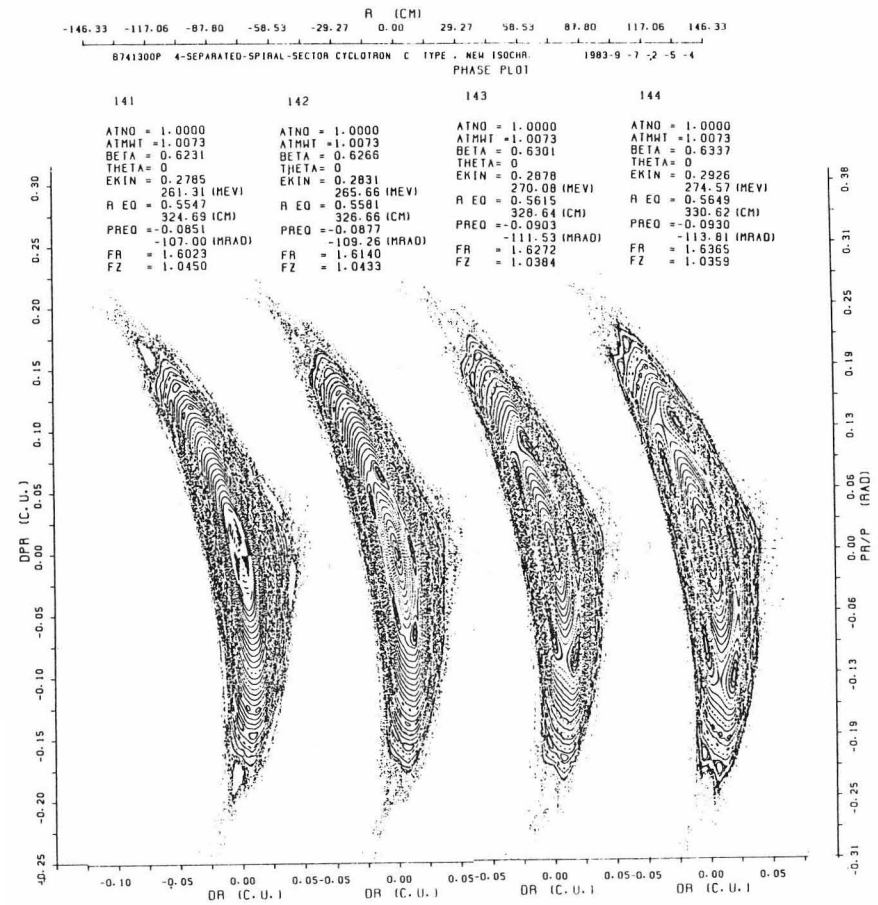

Fig. 7. Phase plots above ν_r=8/5 resonance. Five islands around the equilibrium orbit move outward with energy.

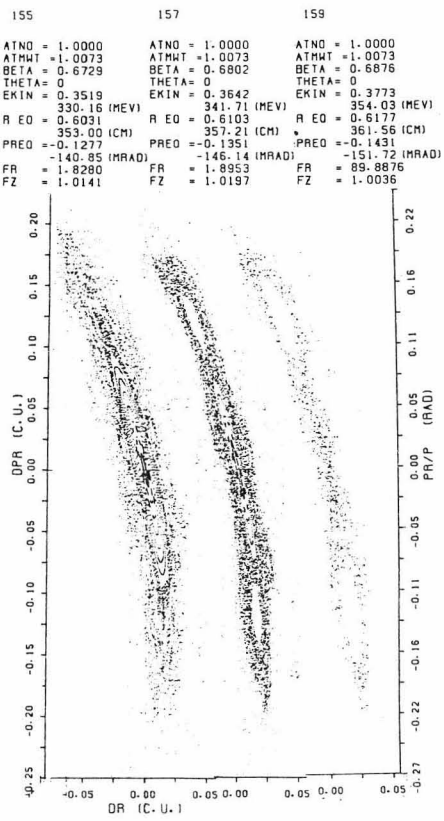

Fig. 8. Phase plots at large radius (1). If the magnetic field is well isochronized to larger radius, the size of the stochastic region becomes larger and two islands due to the stable fixed points of ν=4/2 appear.

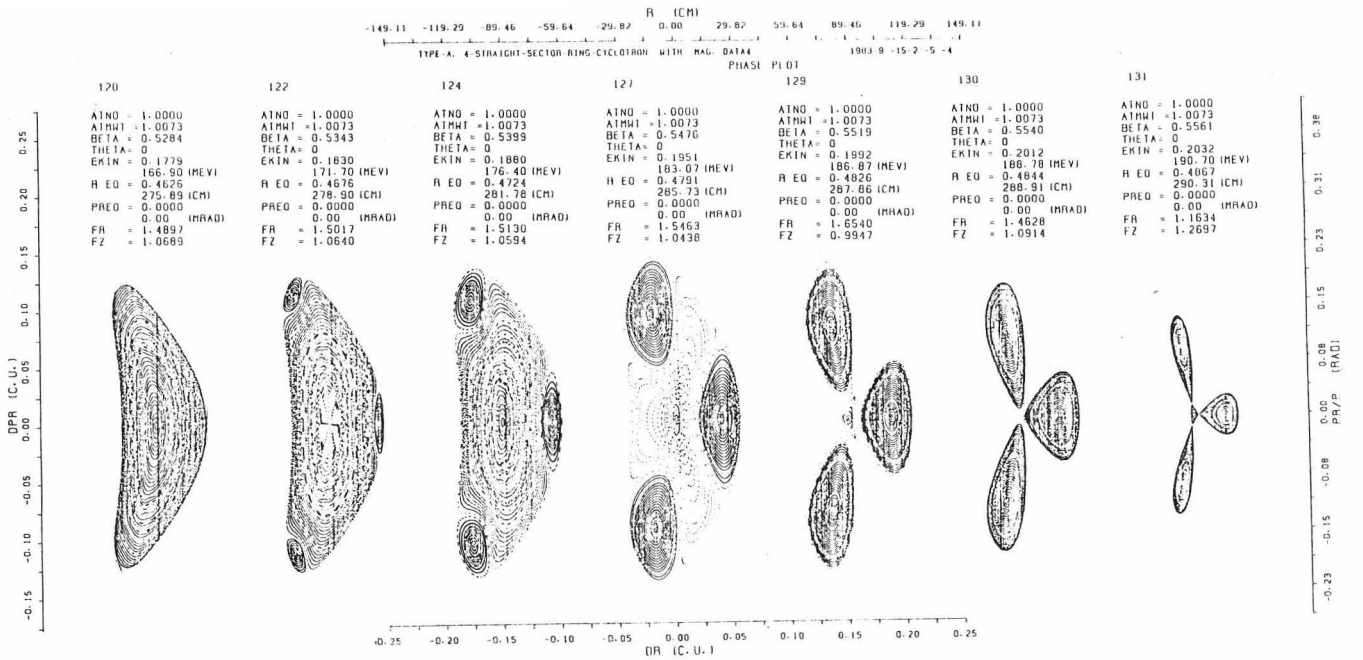

Fig. 9. Phase plots at large radius (2). If the magnetic field is slightly lower than isochronism, three islands due to the stable fixed points of $\nu=4/3$ appears and radial betatron frequency (FR) decreases with energy.

Fig.10. Complicated phase plots.
- a. Outer five islands around the equilibrium orbit are due to the stable points of $\nu=8/5$.
- b. A magnification of the little box in A. The island is surrounded by five small islands.
- c,d. Further magnifications of the small box in B. Figs. c and d show the same phase plots of the same small island with different starting conditions. They show very small islands around the small island.

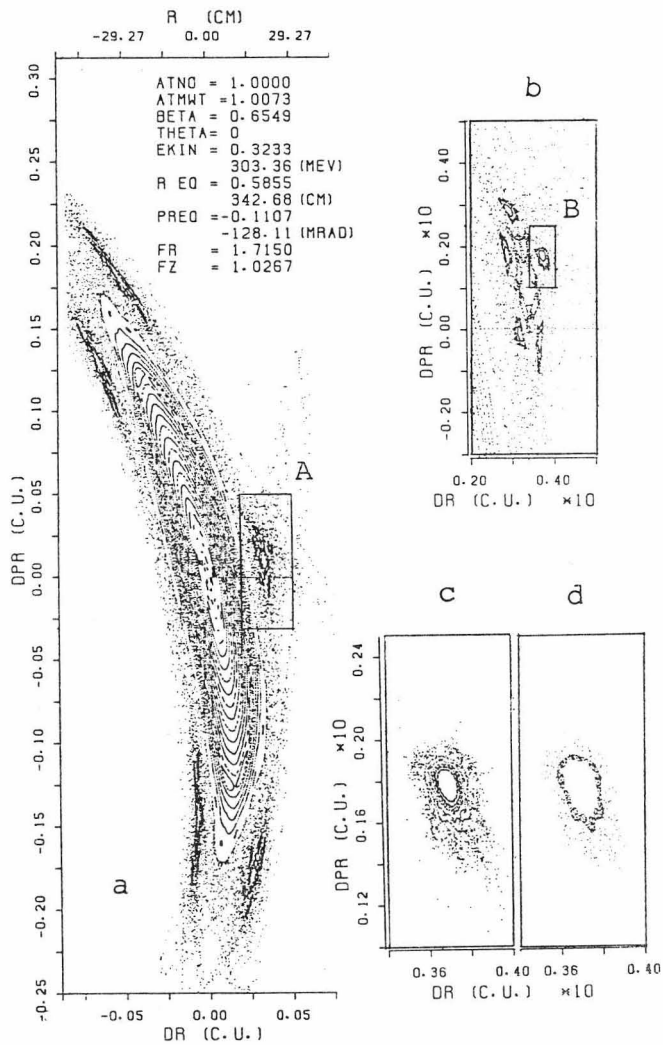

References

1) I. Miura, T. Yamazaki, A. Shimizu, M. Inoue, T. Saito, K. Hosono, T. Itahashi, M. Fujiwara, Y. Fujita and M. Kondo, Proc. Ninth Int. Conf. on Cyclotrons and their Applications, Caen (France) 1981, 89.

2) K. Hosono, I. Miura, T. Itahashi, M. Inoue and A. Shimizu, Porc. Ninth Int. Conf. on Cyclotrons and their Applications, Caen (France) 1981, 379.

3) I. Miura, et al., "A High Energy Version of RCNP Ring Cyclotron" (paper presented at this conference, N4).

4) T. Saito, M. Inoue, A. Shimizu, H. Tamura and I. Miura, Proc. Ninth Int. Conf. on Cyclotrons and their Applications, Caen (France) 1981, 415. T. Saito, et al. "Aluminum RF Cavity for the RCNP Ring Cyclotron" (paper presented at this conference, J13).

* Present address: Okayama University of Science, Okayama 700, JAPAN